

## Heteroatom-Controlled Kinetics of Switchable Polyoxometalate Frameworks

Johannes Thiel, Chris Ritchie, Carsten Streb, De-Liang Long, and Leroy Cronin\*

WestCHEM Department of Chemistry, Joseph Black Building, University of Glasgow, University Avenue, Glasgow G12 8QQ, U.K.

Received December 2, 2008; E-mail: L.Cronin@chem.gla.ac.uk

Modular inorganic frameworks define an exciting new field in coordination chemistry from both the fundamental and applied points of view.<sup>1</sup> This is because these materials have a wide range of applications in catalysis,<sup>2</sup> ion exchange,<sup>3</sup> guest sorption<sup>4</sup> and also serve as model systems for the investigation of structure and bonding, reactivity and dynamic systems.<sup>5</sup> One promising group of building blocks for the design of modular framework compounds are polyoxometalates (POMs), which are anionic oxide clusters of the early transition metals.<sup>6</sup> These compounds combine structural stability and versatility<sup>7</sup> with a wide range of applications in catalysis,<sup>8</sup> medicine<sup>9</sup> and materials science.<sup>6,7</sup> POMs have long been used in the indirect assembly of 3D frameworks,<sup>10</sup> but POM-based framework materials formed by direct connection of the POM clusters (i.e., no exo-cluster linkers) are rare. Recently, we have discovered an archetype of this category.<sup>11</sup> The compound  $(\text{C}_4\text{H}_{10}\text{NO})_{40}[\text{W}_{72}\text{Mn}^{\text{III}}_{12}\text{O}_{268}\text{Si}_7]$  ( $\mathbf{1}_{\text{ox}}$ ) is assembled from Mn-substituted, Si-centered Keggin clusters  $[\text{SiMn}_x\text{W}_{12-x}\text{O}_{40}]$  ( $x = 3-4$ ) that are connected through Mn–O–W linkages. Furthermore, we have shown that the compound can undergo a reversible single-crystal to single-crystal (SC–SC) redox transformation by chemical reduction of the Mn(III) centers with simultaneous unit-cell expansion by 5.48 vol %. This postsynthetic modification switches the electronic properties of the parent material ( $\mathbf{1}_{\text{ox}}$ ) to those of the daughter material  $(\text{C}_4\text{H}_{10}\text{NO})_{40}[\text{H}_{12}\text{W}_{72}\text{Mn}^{\text{II}}_{12}\text{O}_{268}\text{Si}_7]$  ( $\mathbf{1}_{\text{red}}$ ) while retaining the structure of the parent compound  $\mathbf{1}_{\text{ox}}$ .

Herein, we report an extended molecular framework  $(\text{C}_4\text{H}_{10}\text{NO})_{40}[\text{W}_{72}\text{Mn}^{\text{III}}_{12}\text{O}_{268}\text{Ge}_7]$  ( $\mathbf{2}_{\text{ox}}$ ) obtained through a “presynthetic” modification approach in which the overall structural features of the parent compound ( $\mathbf{1}_{\text{ox/red}}$ ) are retained.  $\mathbf{2}_{\text{ox}}$  is obtained using Ge-centered precursors  $[\gamma\text{-GeW}_{10}\text{O}_{36}]^{8-}$  instead of the original Si-centered units  $[\gamma\text{-SiW}_{10}\text{O}_{36}]^{8-}$ .  $\mathbf{2}_{\text{ox}}$  undergoes reversible SC–SC transformations in which the Mn(III) centers are reduced to Mn(II) ( $\mathbf{2}_{\text{red}}$ ) and can be reoxidized to re-form compound  $\mathbf{2}_{\text{ox}}$ . In addition, comparative kinetic studies of these redox transformations show that  $\mathbf{2}_{\text{ox}}$  is reduced faster than  $\mathbf{1}_{\text{ox}}$ . In contrast, the reoxidation of  $\mathbf{2}_{\text{red}}$  proceeds more slowly than that of  $\mathbf{1}_{\text{red}}$ .

Compound  $\mathbf{2}_{\text{ox}}$  was obtained as single crystals by the reaction of  $[\gamma\text{-GeW}_{10}\text{O}_{36}]^{8-}$  with manganese(II) sulfate in a morpholine solution at pH 8.0. After addition of the transition metal salt, the clear solution turned bright-yellow, indicating the presence of manganese(II)-substituted Keggin clusters. Subsequent addition of potassium permanganate to oxidize the manganese(II) centers to manganese(III) resulted in a dark-brown solution from which tetrahedral crystals have been obtained after two weeks.

Structural analysis of the crystals showed that  $\mathbf{2}_{\text{ox}}$  consists of three- and four-connected manganese-substituted, germanium-centered Keggin clusters, which are connected in a 3D framework (Figure 1). The linkages between the clusters are arranged so each three-connected unit only binds to four-connected units and vice versa. Therefore, the trigonal and tetrahedral building blocks are connected by Mn–O–W bridges, where the metal centers are disordered over the two available positions. The clusters form a framework with internal voids, which

are enclosed by four sets of eight-membered rings with diameters of 12.9 Å. The voids themselves are ellipsoidal cavities with dimensions of  $27.17 \times 15.60 \times 8.46$  Å that are partly filled with solvent molecules (~48 H<sub>2</sub>O) and morpholinium cations. Furthermore, the extended 3D structure is topologically identical to that of cubic germanium nitride.<sup>12</sup> After subsequent analysis, the overall formula of  $\mathbf{2}_{\text{ox}}$  was found to be  $(\text{C}_4\text{H}_{10}\text{NO})_{40}[\text{W}_{72}\text{Mn}^{\text{III}}_{12}\text{O}_{268}\text{Ge}_7]$ .

The overall structural features of  $\mathbf{1}_{\text{ox}}$  and  $\mathbf{2}_{\text{ox}}$  are almost identical, the only significant deviation being the coordination geometry of the heteroatoms that template the clusters. The average heteroatom–oxygen distance within the central tetrahedron increases from 1.65 Å (Si–O) to 1.75 Å (Ge–O), which underpins the reactivity difference between the two frameworks.

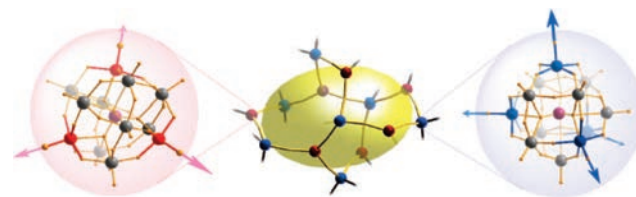
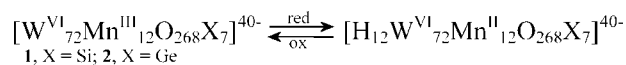


**Figure 1.** Representation of the ellipsoidal voids (middle) in the crystal structures of  $\mathbf{1}_{\text{ox/red}}$  and  $\mathbf{2}_{\text{ox/red}}$ , which are formed by the three- (red spheres) and four-connected (blue spheres) Keggin clusters. Ball-and-stick representations of these building units are shown on the left and right (W, gray and Mn red or blue, respectively; O, orange; Ge/Si, purple).

The chemical reactivity of  $\mathbf{2}_{\text{ox}}$  was investigated by exposing crystals of the compound to a reducing agent; reduction of the material was observed visually as the crystals changed color from dark-brown to bright-yellow while retaining their shape, resulting in the formation of  $(\text{C}_4\text{H}_{10}\text{NO})_{40}[\text{H}_{12}\text{W}_{72}\text{Mn}^{\text{II}}_{12}\text{O}_{268}\text{Ge}_7]$  ( $\mathbf{2}_{\text{red}}$ ) (Figure 2). Subsequently, single-crystal X-ray diffraction (XRD) analysis was performed to investigate the structural integrity of the reduced material. Structural and chemical analysis demonstrated full conversion of  $\mathbf{2}_{\text{ox}}$  to  $\mathbf{2}_{\text{red}}$  with retention of the structure of the parent compound  $\mathbf{2}_{\text{ox}}$  (Scheme 1). However, the reduction of the Mn(III) centers to Mn(II) was reflected by changes in the coordination environment of the Mn-based linkages. The distance between neighboring manganese and tungsten centers increases from 3.592(9) Å in  $\mathbf{2}_{\text{ox}}$  to 3.747(7) Å in  $\mathbf{2}_{\text{red}}$  ( $\Delta = 4.32\%$ ), corresponding to an overall unit-cell volume increase of 4.98 vol % (from 57 774 Å<sup>3</sup> to 60 652 Å<sup>3</sup>). In order to confirm the complete reversibility of the SC–SC redox transformation, hydrogen peroxide was used to reoxidize the crystals of  $\mathbf{2}_{\text{red}}$ . Single-crystal XRD unit-cell checks of the product confirmed the complete transformation back to the oxidized compound  $\mathbf{2}_{\text{ox}}$ . The reduction and reoxidation cycle was repeated three times to demonstrate the stability of the crystalline material.

Initial visual observations of the reductions of  $\mathbf{2}_{\text{ox}}$  and  $\mathbf{1}_{\text{ox}}$  suggested a difference in reaction rates, as a faster color change was observed for the Ge-centered framework  $\mathbf{2}_{\text{ox}}$  than for the original Si-based

## Scheme 1. Reversible Redox Switching of Compounds 1 and 2



compound **1**<sub>ox</sub>. Consequently, it was observed that the reoxidation with hydrogen peroxide proceeds faster for **1**<sub>red</sub> than for **2**<sub>red</sub> (Figure 2).

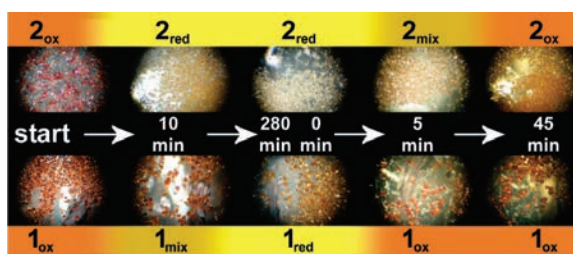


**Figure 2.** Optical micrographs of compounds **1** (bottom) and **2** (top) at various stages of the reduction and reoxidation to visualize the difference in the velocities of the two processes.

To confirm these initial results, a kinetic study in which our initial set of experiments utilized ascorbic acid as a reducing agent was carried out. However, the wide range of oxidation products generated made precise kinetic measurements difficult,<sup>13</sup> so phenylhydrazine was used instead. In order to obtain precise kinetic data, we used an experimental setup where uniformly powdered samples of **1**<sub>ox</sub> and **2**<sub>ox</sub> were used in order to eliminate pore-diffusion issues. In addition, a low concentration of phenylhydrazine in methanol was used for monitoring initial reduction rates to further suppress any systematic errors caused by diffusion effects (compounds **1** and **2** have negligible solubility in methanol). A similar experimental setup was chosen for the reoxidation, and *p*-benzoquinone was employed as an oxidizing agent. This was done to allow for a more precise determination of the rate constants, as the reoxidation with hydrogen peroxide proceeds too rapidly to quantify. In contrast, *p*-benzoquinone allows reaction control and facilitates detection via quantitative UV–vis absorption spectrometry.

The kinetic study of the reductions of **1**<sub>ox</sub> and **2**<sub>ox</sub> with phenylhydrazine under identical conditions showed that in both cases, the concentration of the reducing agent decreases linearly over time (Figure 3, left). This suggests that the rate-determining step can be described by a zero-order rate law, which is often found in heterogeneous systems where the reactive substrate (in this case, **1**<sub>ox</sub> or **2**<sub>ox</sub>) is saturated with the second reagent (in this case, the reducing agent, phenylhydrazine).<sup>14</sup> This rationalization allowed the direct determination of the rate constants ( $k_{\text{ox} \rightarrow \text{red}}$ ) for the two reduction processes. The rate constant found for the reduction of **1**<sub>ox</sub> was determined to be  $k_{1_{\text{ox} \rightarrow \text{red}}} = 40.4 \times 10^{-3}$  (vol ppm) s<sup>-1</sup>. For the reduction of **2**<sub>ox</sub>, the rate constant was  $k_{2_{\text{ox} \rightarrow \text{red}}} = 51.2 \times 10^{-3}$  (vol ppm) s<sup>-1</sup>, which corresponds to an increase of 27% with respect to  $k_{1_{\text{ox} \rightarrow \text{red}}}$ . This is in line with our initial visual observations, which suggested that the reduction of **2**<sub>ox</sub> proceeds considerably faster than the reduction of **1**<sub>ox</sub>. For the reoxidation of the two reduced frameworks, the concentration of the oxidizing reagent *p*-benzoquinone decreases exponentially (Figure 3, right), thus showing first-order reaction kinetics. The kinetic analysis of the reoxidation of **1**<sub>red</sub> gave a rate constant of  $k_{1_{\text{red} \rightarrow \text{ox}}} = 53.0 \times 10^{-3}$  s<sup>-1</sup>. The slower reoxidation of **2**<sub>red</sub> is reflected by the correspondingly lower rate constant,  $k_{2_{\text{red} \rightarrow \text{ox}}} = 42.9 \times 10^{-3}$  s<sup>-1</sup>. This means that  $k_{1_{\text{red} \rightarrow \text{ox}}}$  is 24% larger than  $k_{2_{\text{red} \rightarrow \text{ox}}}$ , in support of our initial findings. We hypothesize that the differences between the redox kinetics of **1** and **2** can be related to the electrochemical properties of the discrete Keggin cluster units. The faster reduction of compound **2**<sub>ox</sub> compared with **1**<sub>ox</sub> is in accordance with the reduction potentials of manganese-substituted

$\alpha$ -Keggin heteropolytungstates. In the case of  $[\text{XMn}^{\text{III}}(\text{OH})_2\text{W}_{11}\text{O}_{39}]^{5-6-}$  (X = Si, Ge), the reduction potential for the Mn(III) → Mn(II) reduction step is  $E^0 = +0.81$  V for the Ge-centered cluster. In comparison, the Si-centered cluster gives a reduction potential of  $E^0 = +0.61$  V,<sup>15</sup> suggesting an easier reduction and slower reoxidation of the manganese centers when germanium is utilized.

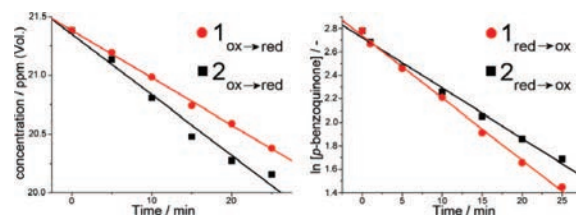


**Figure 3.** Kinetic measurements for the determination of the rate constants for reduction (left) and reoxidation (right).

In conclusion, we have demonstrated that it is possible to construct framework architectures that undergo controlled reversible SC–SC redox transformations, where the kinetics of the processes are controlled by the redox agent and the heteroatom cluster template. These studies show that it is possible to modify the overall structure of compounds **1** and **2** by a redox-based “postsynthetic” modification. Furthermore, we are also able to change the chemical properties of the POM frameworks by substituting the heteroatom in the building units in a “presynthetic” modification. The surprising redox properties of frameworks **1** and **2** demonstrate how functional systems can be developed, allowing reactivity control using pre- and postsynthetic modifications of isostructural frameworks. This opens up a plethora of applications whereby redox-tunable frameworks such as those presented here could be applied as sensors or catalysts. In the future, we will develop this range of materials and explore the dynamics of the redox transformations as well as try to use the isostructural frameworks for selective reactions as a function of the electronic state of the materials.

**Acknowledgment.** The authors thank the EPSRC, the University of Glasgow, WestCHEM, and the Leverhulme Trust for support.

**Supporting Information Available:** Experimental details (including synthesis and characterization) and X-ray crystallographic data (CIF) for **2**<sub>ox/red</sub>. This material is available free of charge via the Internet at <http://pubs.acs.org>.

## References

- (1) Yanai, N.; Uemura, T.; Ohba, M.; Kadowaki, Y.; Maesato, M.; Takenaka, M.; Nishitsui, S.; Hasegawa, H.; Kitagawa, S. *Angew. Chem., Int. Ed.* **2008**, *47*, 9883.
- (2) Cho, S.-H.; Ma, B.; Nguyen, S. T.; Hupp, J. T.; Albrecht-Schmitt, T. E. *Chem. Commun.* **2006**, 2563.
- (3) Cheetham, A. K.; Férey, G.; Loiseau, T. *Angew. Chem., Int. Ed.* **1999**, *38*, 3268.
- (4) Eddaoudi, M.; Li, H.; Yaghi, O. M. *J. Am. Chem. Soc.* **2000**, *122*, 1391.
- (5) Kawamichi, T.; Kodama, T.; Kawano, M.; Fujita, M. *Angew. Chem., Int. Ed.* **2008**, *47*, 8030.
- (6) Müller, A.; Roy, S. *The Chemistry of Nanomaterials: Synthesis, Properties and Applications*; Wiley-VCH: Weinheim, Germany, 2004.
- (7) Long, D.-L.; Burkholder, E.; Cronin, L. *Chem. Soc. Rev.* **2007**, *36*, 105.
- (8) Mizuno, N.; Misono, M. *Chem. Rev.* **1998**, *98*, 199.
- (9) Rhule, J. T.; Hill, C. L.; Judd, D. A. *Chem. Rev.* **1998**, *98*, 327.
- (10) Song, Y.-F.; Long, D.-L.; Cronin, L. *Angew. Chem.* **2007**, *119*, 3974.
- (11) Ritchie, C.; Streb, C.; Thiel, J.; Mitchell, S. G.; Miras, H. N.; Long, D.-L.; Boyd, T.; Peacock, R. D.; McGlone, T.; Cronin, L. *Angew. Chem., Int. Ed.* **2008**, *47*, 6881.
- (12) Kroll, P. *J. Solid State Chem.* **2003**, *176*, 530.
- (13) Koliou, E. K.; Ioannou, P. V. *Carbohydr. Res.* **2005**, *340*, 315.
- (14) Kang, H. C.; Weinberg, W. H. *Chem. Rev.* **1995**, *95*, 667.
- (15) Tourné, C. M.; Tourné, G. F.; Malik, S. A.; Weakley, T. J. R. *J. Inorg. Nucl. Chem.* **1970**, *32*, 3875.

JA809422K